Chapter 2

Iron oxide model catalysts: a surface science approach towards styrene synthesis

2. The Model catalysis approach

2.1 Introduction

Here, I will try to review the model catalysis approach applied to the investigation of the catalytic dehydrogenation of EB to St which has been done so far in our research group over unpromoted and potassium-promoted iron oxide model catalysts. The catalyst is complex. Since the divalent Fe^{2+} and the trivalent Fe^{3+} state are similarly stable, there exist several stable or meta-stable oxide phases. Addition of K produces several stable or meta-stable ternary KFe_xO_y phases [1].

The idea is not new to overcome the pressure gap by combination of a conventional UHV chamber with a high-pressure cell [56-58]. Preparation and characterization of a catalytically interesting surface is performed in UHV using the methods of surface science and after that the sample is transferred under vacuum into a high-pressure cell where catalytic conversion measurements can be performed at pressures far enough away from UHV to yield information relevant to real catalysis conditions.

The basic idea of model catalysis as we apply it is to prepare well defined model catalyst samples and to characterize their surface structure and composition as well as their adsorption-desorption properties for the relevant gases. Then the samples are transferred under vacuum into a reactor which allows determining the catalytic properties (conversion, selectivity, deactivation behaviour) in-situ under realistic temperature and pressure conditions. After that, the samples are transferred back into the main UHV chamber for post-reaction analysis [74].

2.2 Preparation and characterization of iron oxide thin films.

2.2.1 Geometric surface structures and stability ranges of iron oxides

A number of different phases with different stoichiometries and crystal structures were prepared from iron and oxygen (the detailed preparation procedure is explained in the experimental chapter 3) these phases are: FeO (wustite), Fe_3O_4 (magnetite) and α-Fe_2O_3 (hematite), which occur naturally. Under thermodynamic equilibrium their stability ranges depend on the ambient oxygen gas pressure $p(O_2)$ and on the temperature T. These stability ranges for pressures below 1 bar are shown in the phase diagram for the iron-oxygen system in Fig. (2.1) [59,61]. It was calculated using commercial software [60] for $p(O_2)$-T ranges used in the preparation of the iron oxide model catalyst films.

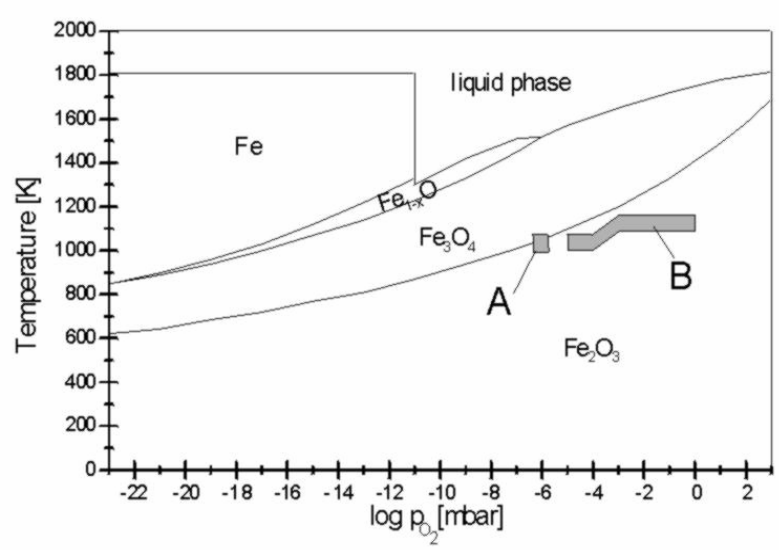

Fig. (2.1). $p(O_2)$-T phase diagram of the iron-oxygen system. The ranges where Fe_3O_4 (A) and Fe_2O_3 (B) films were grown on Pt(111) are indicated.

Fig. (2.2) shows a perspective side and top views of the three iron oxide crystal structures studied extensively earlier in our group [74]. They expose surface planes as

obtained by truncating the bulk structure. The side views show the hexagonal iron and oxygen (111) and (0001) planes stacked consecutively along the [111] and [0001] crystal directions, the top views show the unreconstructed (111) and (0001) surfaces terminated by topmost iron layers. The two-dimensional surface unit cells are also indicated.

FeO wustite crystallizes in the sodium chloride structure containing four formula units in the cubic unit cell. The large O^{2-} anions form a close packed fcc sublattice with the small Fe^{2+} cations located in the interstitial sites. All iron ions are octahedrally coordinated to oxygen. Under thermal equilibrium this phase is stable only at low pressures (Fig. (2.1)) and for temperatures above 843 K [64]. In this oxide the oxygen and iron (111) planes form ideal two-dimensional hexagonal lattices with an inter-atomic distance of 3.04 Å, which corresponds to the lattice constant of the hexagonal unit cell on the unreconstructed FeO(111) surface. Along the [111] direction the iron and oxygen (111) planes form the cubic ABC stacking sequence with an interlayer distance of 1.25 Å. The iron-oxygen bond length is 2.16 Å.

Fe_3O_4 magnetite is ferromagnetic and crystallizes in the inverse spinel structure [62]. The oxygen anions form a close-packed fcc sublattice with Fe^{2+} and Fe^{3+} cations located in the interstitial sites. One cation site is tetrahedrally coordinated to oxygen and is occupied only by Fe^{3+} ions. The other site is octahedrally coordinated to oxygen and is occupied by equal numbers of Fe^{2+} and Fe^{3+} ions. The cubic unit cell has a lattice constant of 8.396 Å and contains eight formula units which can be written as $(Fe^{3+})_8[Fe^{3+}\ Fe^{2+}]_8O_{32}$. The parentheses ( ) denote the tetrahedrally coordinated Fe^{3+} ions, often labeled A sites, and the brackets [ ] denote the octahedrally coordinated Fe^{2+} and Fe^{3+}

ions or B sites. The high electrical conductivity of magnetite at room temperature is attributed to electron hopping processes between the Fe^{2+} and Fe^{3+} ions.

Along the [111] axis of Fe_3O_4 the hexagonal oxygen planes form a cubic ABC stacking sequence. Between the oxygen (111) planes one Kagomé, three hexagonal (mix-trigonal) iron layers alternate. In the Kagomé layer ¾ of the octahedrally coordinated B sites are occupied by Fe^{2+} and Fe^{3+} species. The unoccupied sites in these planes are 5.94 Å apart forming an ordered hexagonal lattice. In the mix-trigonal layers only ¼ of all sites are occupied within each subplane: The central plane contains octahedrally coordinated Fe^{3+} and Fe^{3+} species located on B sites, the other two planes tetrahedrally coordinated Fe^{3+} species located on A sites. The interatomic iron-iron distance within these planes is also 5.94 Å, which corresponds to the lattice constant of the two-dimensional surface unit cell of $Fe_3O_4(111)$ indicated in Fig. 2.2. There is a slight deviation of the oxygen anion positions within the (111) planes from an ideal hexagonal arrangement of this surface, due to two types of oxygen anions which are denoted O_a and O_b in Fig. (2.2). The O_a species are located 0.04 Å closer to the topmost single octahedrally coordinated iron layers than the O_b species. The average oxygen-oxygen interatomic distance within the (111) planes is 2.97 Å. If we consider weighted values for the O_a and O_b sublayers, neighboring oxygen (111) planes separated by the Kagomé layer are 2.37 Å apart, oxygen planes separated by the three mix-trigonal layers are 2.48 Å apart. This leads to a distance of 4.85 Å between every second oxygen layer, which corresponds to the distance between equivalent (111) surface terminations of Fe_3O_4. The iron sub-planes of the mix-trigonal iron layers are separated by 0.6 Å. The iron-oxygen

bond lengths for tetrahedrally coordinated iron is 1.88 Å, that for octahedrally iron is 2.07 Å. The (111) surface plane is stable and frequently occurs on naturally grown crystals which assume octahedral shapes [64].

α-Fe_2O_3 hematite is the only iron oxide phase that is stable at room temperature in thermodynamic equilibrium with ambient oxygen atmospheres. It crystallizes in the corundum structure with the hexagonal unit cell containing six formula units. The lattice constants are a=5.035 Å and c=13.72 Å [64]. The oxygen anions form an hcp sublattice with ABAB stacking. The Fe^{3+} species in the interstitials are arranged in distorted octahedra and form two sublayers. The interatomic distance within these iron layers is 5.03 Å, which corresponds to the lattice constant of the two-dimensional unit cell of an unreconstructed (0001) surface, as indicated in the top view of Fig. (2.2). The oxygen anion positions within the (111) planes also deviate slightly from an ideal hexagonal arrangement. The average oxygen-oxygen interatomic distance is 2.91 Å. Due to the distortion of the octahedra there are two different iron-oxygen bond lengths, 1.96 Å and 2.09 Å. The two iron subplanes in-between the oxygen planes are separated by 0.6 Å. The distance between two oxygen planes is 2.29 Å, which corresponds to the distance between equivalent (0001) surface terminations.

The quasi-hexagonal surfaces of the three iron oxide phases in Fig. (2.2) form three different unit cells provided no reconstructions occur. They have lattice constants of 3.04 Å (FeO), 5.92 Å (Fe_3O_4) and 5.03 Å (α-Fe_2O_3). The α-Fe_2O_3(0001) unit cell is rotated by 30° with respect to the others. Therefore the LEED patterns of these surfaces can be used to identify the different iron oxide phases.

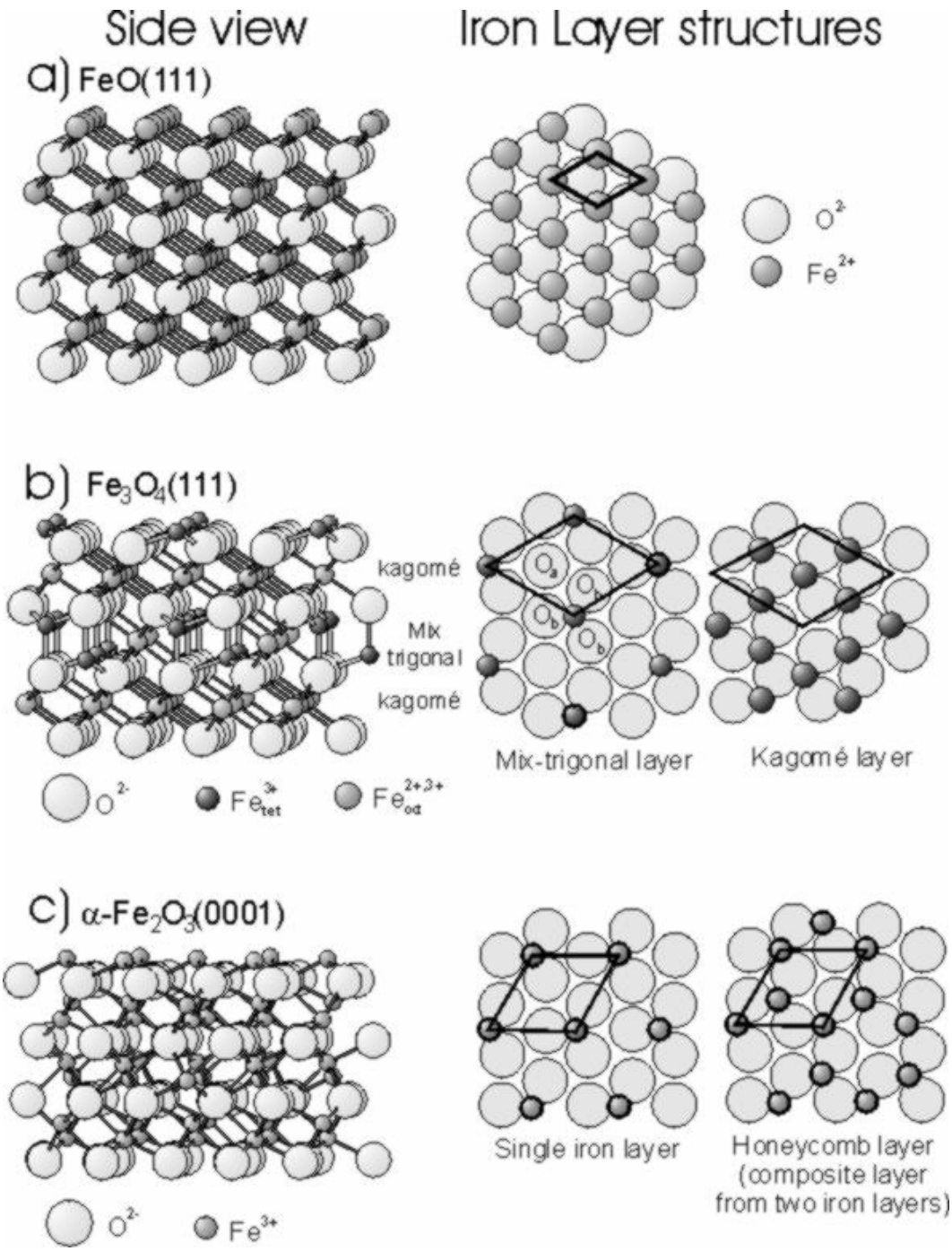

Fig. (2.2). Perspective side views of iron oxide crystal structures and top views cut parallel to the close packed oxygen layers. Bulk truncated (111) and (0001) surface structures terminated by outermost iron planes are shown. The surface unit cells are indicated. The top views are drawn with the full cation and anion sizes. In the side views the ionic radii were reduced by a factor of two.

2.2.2 Potassium-Iron oxide compounds: structures and stability ranges

Several ternary compounds containing both iron oxides and potassium are described in literature like $KFeO_2$ [67], and various phases with the general composition $K_2O*nFe_2O_3$ (n=2, 5, 6, 7, 11). Very likely, these compounds are mixtures of hexagonal phases with ideal compositions $K_2Fe_4O_7$, $K_2Fe_{22}O_{34}$ and $K_4Fe_{22}O_{34}$. The formation of $KFeO_2$ in the technical catalyst was found to proceed with a high yield between 873-1073 K while the transformation of $KFeO_2$ to $K_2Fe_{22}O_{34}$ (k-α-Fe_2O_3) starts around 1023 K. All results in literature suggests that the ternary phases $KFeO_2$ and $KFe_{22}O_{34}$ (x=2.4) may occur as stable phases when K_2O and Fe_2O_3 are brought into contact. Similar results are expected when potassium is deposited on Fe_3O_4 and annealed. Stability regions of these ternary compounds also in dependence of the water partial pressure were investigated in our group [22], It showed that below a phase boundary ranging from 447 K at 10^{-11} mbar to 626 K at 10^{-5} mbar, KOH is formed while beyond this phase boundary KOH decomposes and potassium desorbs into the gas phase.

Potassium-promoted thin films were prepared and studied earlier [72,73]. K was deposited using a SAES getter source on Fe_3O_4 or Fe_2O_3 films, followed by annealing in vacuum or at $p(O_2)=10^{-6}$ mbar. The most stable K-Fe-O phases are the K-rich $KFeO_2$ (K-ferrite) and the K-poor $K_xFe_{22}O_{34}$ with x=2 (K-β-ferrite) or x=4 (K-β''-ferrite). $K_xFe_{22}O_{34}$ has a hexagonal layer structure which can be considered as a sequence of spinel-like blocks $–(O_4\text{-}Fe_3)_3\text{-}O_4$- etc. as in Fe_3O_4, separated by -Fe-K_xO-Fe- layers. Lower K-contents (x<2) can be achieved either by increasing the thickness of the spinel blocks, thus continuously approaching the pure Fe_3O_4, or by a decrease in the occupation

of the potassium sublayers. Because of the similarity of the spinel blocks with the Fe_3O_4 spinel structure, the lattice constant of the $K_xFe_{22}O_{34}(0001)$ and $Fe_3O_4(111)$ surfaces are almost identical and epitaxial growth is easy. $KFeO_2$ is tetragonal without any layered character and does not fit with the lattice of Fe_3O_4. In its bulk, the K, Fe and O atoms are quite homogeneously distributed. A structure model for $K_2Fe_{22}O_{34}$ (a) and $KFeO_2$ phases (b) is shown in Fig. (2.3).

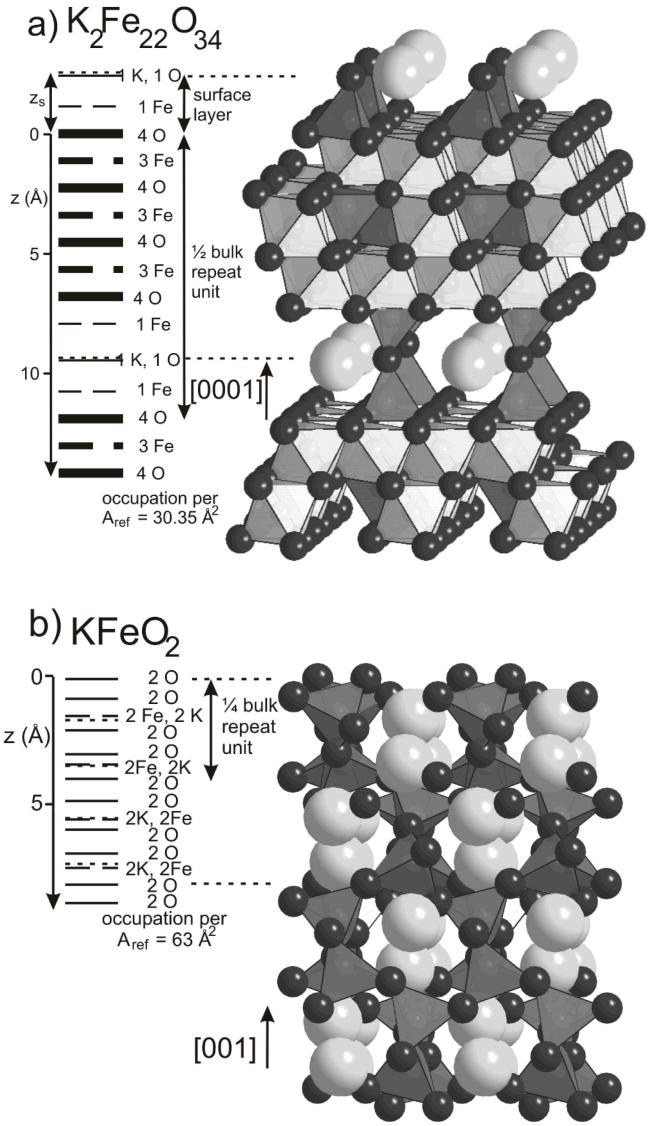

Fig. (2.3) Structure models and layer arrangement for the ternary compound $K_2Fe_{22}O_{34}$ (a) and $KFeO_2$ (b). K is the large gray balls, O is the small dark balls and the Fe atoms are located in the center of the octahedral and the tetrahedral.

The preparation conditions, composition and stability of these phases have been mapped using XPS, AES, which allows the quantitative determination of the elemental composition within the analysis depth of about 25 Å [72,73]. The most important composition steps observed when a thick layer of K is deposited on a Fe_3O_4(111) thin film at 200 K and annealed stepwise up to 970 K are the following :

- At 700 K a uniform $KFeO_2$ phase has formed.
- At 800-900 K, a layered structure has formed with a thin $KFeO_2$ layer structure on the top of a K-poorer $K_xFe_{22}O_{34}$ phase (0>x>2). The analogy with the layered structure of the working real catalyst as proposed by Muhler [15,22] is sticking.
- At 970 K, a well ordered $K_xFe_{22}O_{34}$ (0001)-(2x2) phase ($x \leq 0.67$) is left.
- Beyond 700 K, addition of H_2O accelerates the removal of potassium from the films considerably.

2.3 Surface structure characterization:

2.3.1 (LEED and STM)

Fig. (2.4) shows the LEED patterns, STM images and surface structure models of those model catalyst layers which form ordered surfaces. The hexagonal oxygen layers are very similar in all cases with O-O distances varying only between 0.290 nm in Fe_2O_3, 0.296 nm in Fe_3O_4 and $K_xFe_{22}O_{34}$ and 0.304 nm in bulk FeO. The thin FeO layers on Pt have expanded lattice constants. The strong differences in the LEED patterns and the STM images result therefore from the different arrangement of the Fe atoms between the

oxygen layers. Typical for the quite thin FeO(111) layers (shown is a film only one Fe-O bi-layer thick) are the satellite patterns around the integral order spots in LEED and the Moiré pattern of the STM image. Both are a result of the low film thickness and the misfit between the Pt(111) and the FeO(111) lattice. The satellite spots result from multiple scattering involving the Pt and FeO lattice. The Moiré pattern reflects the different positions of the Fe atoms on the Pt lattice, periodically changing between on-top, bridge and threefold hollow site positions. All three kinds of sites occur in the shown structure because the FeO layer is rotated with respect to the Pt substrate. Photoelectron diffraction studies [74] have shown that the surface is oxygen terminated. However, the bright dots in STM reflect the positions of the Fe atoms underneath which show both unoccupied and occupied levels near the Fermi level [74]. For details of the structure see ref. [74].

The Fe_3O_4(111) surface has a threefold symmetry. Mostly, however, two domains rotated by 60° with respect to each other are equally distributed so that the LEED pattern has six-fold symmetry. As for FeO, the STM image reflects the surface unit cell. Again, the bright spots correspond to surface Fe atoms. They are quite clear on Fe_3O_4(111) because this surface Fe forms the top layer as proven by a LEED structure analysis and indicated in the model.

The surface unit cell of α-Fe_2O_3(0001) is again different. The STM image is again formed by Fe derived spots but the contrast is lower than on Fe_3O_4. The reason is that the surface is oxygen-terminated or possibly even hydroxylated as a LEED structure analysis has shown [74]. Also the decrease in the intensity of the spots or there broadening and the

high background in the LEED images gave and indication of the increase of the surface roughness or disorder [61].

Depending on the amount of deposited K and the annealing temperature, different ternary K-Fe-O compounds are formed. Already at 300 K, the deposited K diffuses into the bulk and at 700 K, the K-rich $KFeO_2$ phase forms uniformly as concluded from quantitative XPS measurements [73]. It has, however, no long-range order and no LEED patterns are formed [72].

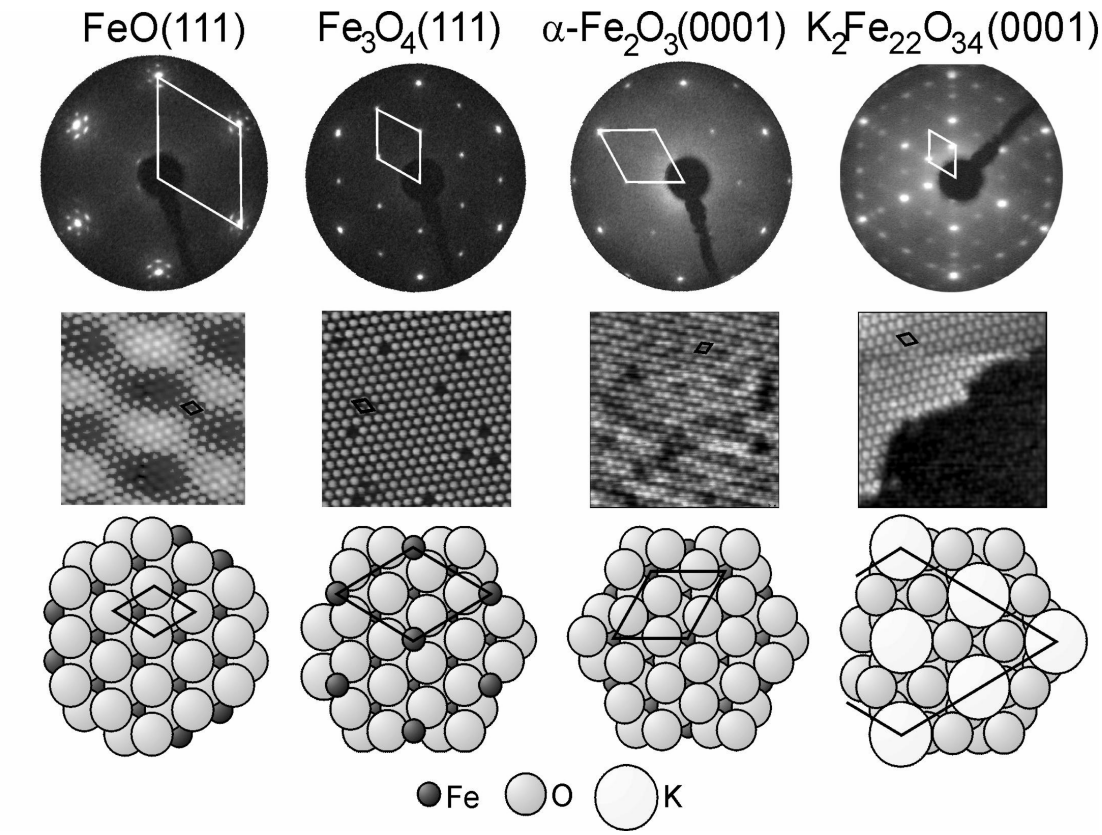

Fig.(2.4). LEED patterns at E=60 eV and top views of the corresponding surface structures of the Pt(111) substrate (a), and of the different iron oxide films grown onto Pt(111) (b) to (d). The unit cells in real and reciprocal space and the crystallographic directions in the cubic (a-c) and hexagonal crystal structures (d) are indicated. The epitaxial relationships between the oxide films and the substrate surface lattice are reflected in this figure.

STM imaging is difficult and only possible on a very thin (2 nm) film because of the insulating character of this compound. The film is rough and atomic resolution was not achieved [73]. When annealing between 800 and 900 K, potassium is slowly removed from the film (the speed increases strongly when water is present) in the way that a $KFeO_2$ layer of decreasing thickness remains at the surface while the underlying film converts to $K_xFe_{22}O_{34}$. The $KFeO_2$ disappears completely at 970 K and a $K_xFe_{22}O_{34}$ layer is left. The XPS results [73] suggest that the surface is terminated by a complete Fe-K-O layer while the bulk contains less potassium, corresponding to about $x \approx 0.67$. This is then the only KFe_xO_y layer with good long-range order. Its LEED pattern and STM image are shown in Fig. (2.4).

2.3.2 AES measurements

AES provides element-specific information on the surface region of the studied model catalyst. Fig. (2.5) shows AES spectra of the three iron oxide films, no contamination signals are seen here. An AES spectrum for Fe_3O_4 after reaction in the micro flow reactor is shown also, where the carbon deposits are clearly seen on the thin film surface. The AES peak intensity ratios of $\mathbf{I}_K$, $\mathbf{I}_O$, $\mathbf{I}_C$ with respect to $\mathbf{I}_{Fe}$ are used for comparison of surface composition changes of the different model catalysts. As expected, the α-Fe_2O_3 film has a higher oxygen/iron intensity ratio ($\mathbf{I}_O/\mathbf{I}_{Fe}$) than the Fe_3O_4 film. Potassium promoted catalysts (potassium signal appears at 256 eV) with different potassium loading are differentiated by the intensity ratio of potassium/iron ($\mathbf{I}_K/\mathbf{I}_{Fe}$) and compared to the β-

Ferrite-$K_xFe_{22}O_{34}$(0001) which has a 2x2 LEED pattern and a moderate potassium content of ($\mathbf{I}_K/\mathbf{I}_{Fe}$~2.7) (Fig. (2.5b)).

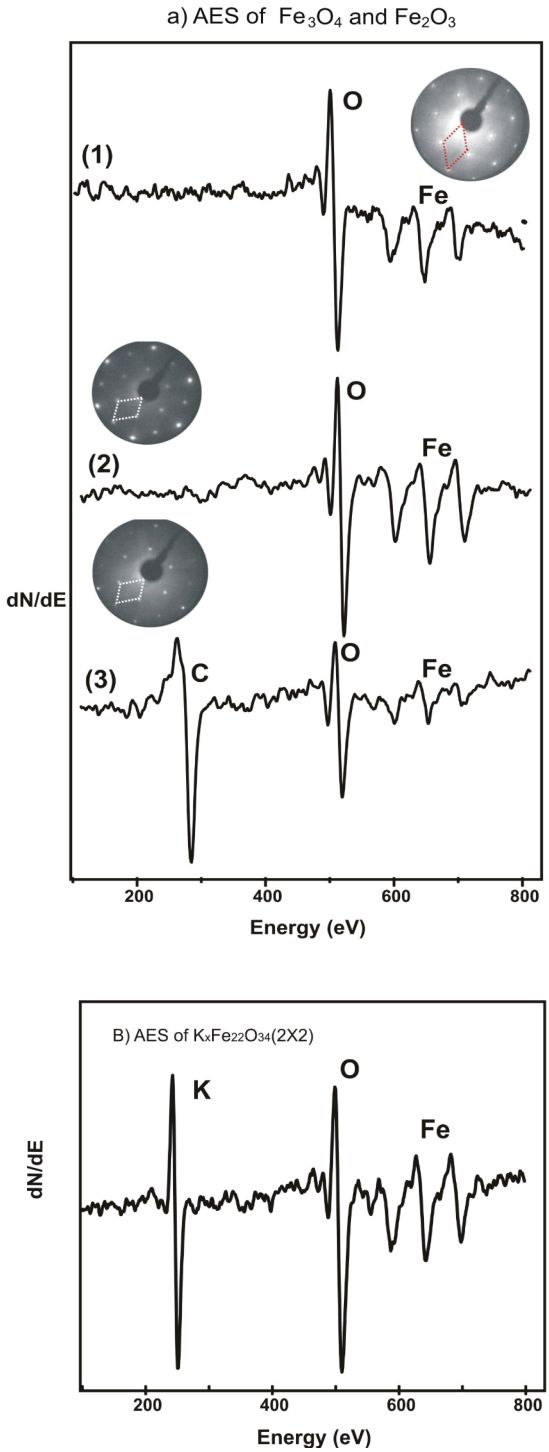

Fig. (2.5).
a) AES spectra of epitaxial iron oxide films grown onto Pt(111).
(1)the a-*Fe_2O_3(0001),*
(2) Fe_3O_4(111) before reaction
(3) Fe_3O_4(111) after reaction,
b) KFe_xO_y films are at least 100 Å thick.

2.3.3 Adsorption properties (TDS, UPS and NEXAFS)

A great deal of work has been spent on the determination of the surface structure using LEED-(I-V) measurements in combination with dynamic structure analysis calculations [63,75,76], on the determination of the kind of adsorbed species (molecular or dissociated) after exposure to EB[77], St [78] and H_2O using UPS, on the adsorbate orientation using NEXAFS [79] and on the energetic and kinetic data for adsorption and desorption using TDS and isosteric methods [78]. The collected knowledge for EB and St is summarized in Fig. (2.6a).

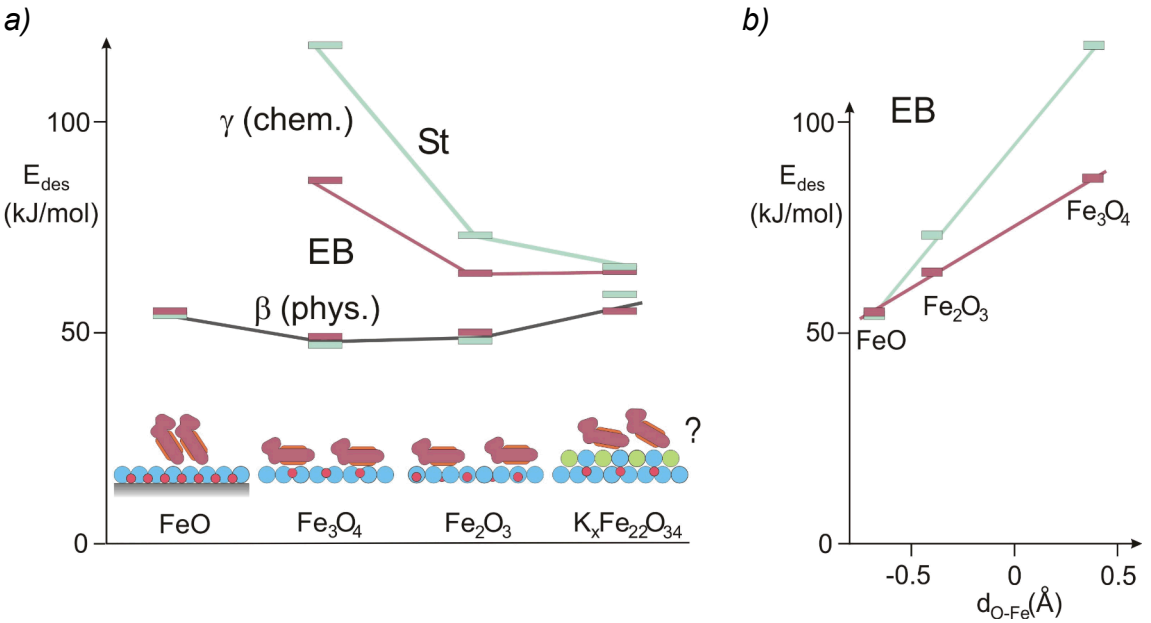

Fig. (2.6). Energetic and structural results for EB (filled symbols) and St (open symbols) adsorption on different substrate films. (a) Desorption energies from TDS [74] for chemisorbed (g) and physisorbed (b) species and adsorbate arrangement at low coverages of the initially adsorbing species (b on FeO, g on the others). Shown is adsorbed EB, the arrangement for St is similar. Adsorbate structure for Fe_xO_y from NEXAFS measurements [74]. The arrangement on $K_xFe_{22}O_{34}$ is hypothetical. (b) Dependence of the desorption energy for the initially adsorbing species on the position of the first iron layer relative to the first oxygen layer.

The FeO film is O-terminated. The first Fe layer is relatively deep below the O-layer (-0.068 nm [83] or 0.062 nm [84]). Also Fe_2O_3 is O-terminated but according to the best-fit structure [59], the first Fe layer is only 0.046 nm below the surface O-layer. In contrast, Fe_3O_4 is Fe-terminated. The Fe atoms are +0.038 nm above the first O-layer. This has a decisive influence on adsorbate structure and interaction. UPS shows all adsorbate states of EB and St at room temperature and below are molecular. NEXAFS shows that for FeO that EB and St adsorb strongly tilted from the beginning. The only adsorbate state is a weakly bound physisorbed state. Although there is no direct evidence for island formation of the adsorbate, It is likely that the adsorbate-substrate interaction is so weak that adsorbate-adsorbate interaction dominates. As characteristic for condensed aromatics, this interaction probably occurs via the π-orbitals of the benzene ring so that the molecules get tilted. In contrast, both EB and St adsorb almost flat on Fe_3O_4 and Fe_2O_3, at least for low coverages. Near saturation, tilting increases due to increasing adsorbate-adsorbate interaction. Flat adsorption correlates with the existence of chemisorbed γ-states which saturate before a second, physisorbed layer forms. Chemisorption is much stronger on Fe_3O_4 than on Fe_2O_3, and it is stronger for St which has a conjugated π-system extending also over the ethyl group, at least if it adsorbs in a planar configuration.

UPS measurements for EB on Fe_3O_4 in adsorption-desorption equilibrium show that saturation of the chemisorbed γ-state corresponds to one EB molecule on two Fe surface sites. This corresponds to only about 83 % of a close-packed adsorption layer assuming a flat adsorbate configuration (Van-der-Waals area of EB ~0.5 nm^2). The physisorbed first

β-layer on FeO, however, saturates at a full monolayer which rules out a correlation of the adsorbate with the surface structure [80,81].

These results prove that chemisorption is dominated by the interaction between the strongly polarizable π-system of the adsorbate which represent a soft base [82] and the acidic Fe ions. This is highlighted by Fig. (2.6b) which gives the dependence of E_{des} for the initially adsorbing species (β for FeO, γ for Fe_2O_3 and Fe_3O_4) on the Fe-layer position with respect to the O-layer. On Fe_2O_3, the Fe-layer is relatively deep below the O-layer but the molecules can obviously still "feel" it and arrange in a flat chemisorbed state. Although the Fe-layer is not much deeper on FeO, the interaction is too weak to compete with the Van-der-Waals interaction between the adsorbates.

For the $K_xFe_{22}O_{34}$ film, a structure analysis does not exist. The quantitative XPS results [73] are compatible with a termination by a Fe-K-O layer as in the bulk of $K_2Fe_{22}O_{34}$. In this case, the first Fe atoms are below the O atoms of the top layer and an interaction with the adsorbate would be weak. On the other hand, interaction may occur with surface K ions, but as long as a structure analysis is missing, any adsorption model is speculative. The existence of a chemisorbed state which proceeds physisorption and has similar binding energies as on Fe_2O_3 suggests that the binding situations on these two surfaces are similar. The difference of the bond strength for EB and St has almost disappeared.

2.3.4 Catalytic activity (Low and medium pressure reactivity measurements)

The first reactivity measurements were performed on unpromoted model catalysts using mass spectrometric analysis in the main UHV chamber by Zscherpel et.al. [85]. A mixture EB:H_2O=1:5 at a total pressure of 3.5×10^{-6} mbar was applied. It turned out that well ordered Fe_2O_3 hematite samples with sharp spots and low background in the LEED pattern were quite inactive while poorly ordered samples with broad spots and high background clearly showed conversion. Typical mass spectrometer traces are presented in Fig. (2.7) [85]. The sample was kept at 873 K, water was admitted at t=0, EB about 20 – 30 s later. On a poorly ordered active Fe_2O_3 film, deactivation was observed after several such cycles, going along with indications for reduction to Fe_3O_4 in the LEED pattern. Also carbonaceous deposits were detected by in-situ photoelectron emission microscopy (PEEM). Fe_3O_4 samples were inactive, irrespective of the surface order.

In a first attempt to bridge the pressure gap, medium pressure batch reactor experiments were performed. The high pressure chamber (Fig. (2.8)), at that time without reactor) was used as batch reactor cell. For mass spectrometric analysis, a bypass line with a dosing valve was mounted between the high pressure chamber and the UHV analysis chamber. The gas mixture (EB:H_2O=1:10, total pressure 0.6 mbar) was admitted and after about 10 min, sample heating was started. After a few minutes, the reaction temperature was reached. Fig. 8 shows that styrene and hydrogen evolution goes along with ethylbenzene consumption. Again, activity increases with the degree of disorder of the starting Fe_2O_3 film. The most active film was deactivated after about 30 min. PEEM showed coke deposits. In AES, carbon was visible and after its removal by a mild oxidation cycle,

LEED showed a mixture of the patterns of Fe_2O_3 and Fe_3O_4, confirming catalyst reduction during the experiment. Corresponding experiments using Fe_3O_4 model catalysts again showed no measurable activity.

These experiments showed that meaningful conversion measurements can be performed over single crystal samples with a surface area of as little as 0.5 cm^2. They confirmed that Fe_2O_3 is clearly more active than Fe_3O_4. Deactivation of Fe_2O_3 goes along with reduction and coking and defects are necessary for high conversion.

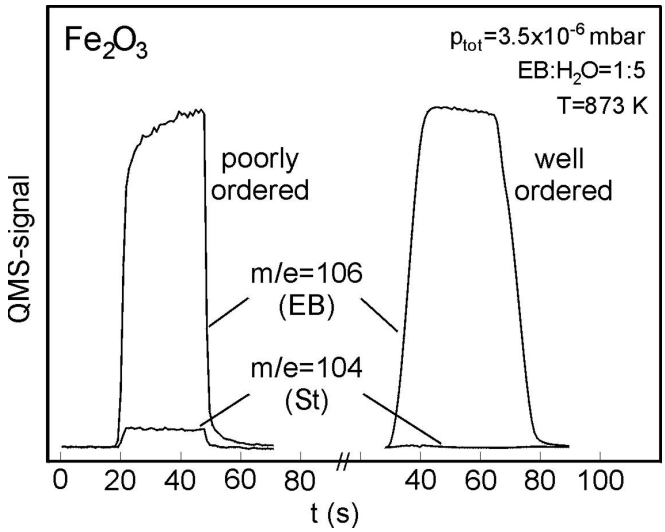

Fig. (2.7).

Mass spectrometer traces for EB and St under low pressure reaction conditions as indicated over poorly ordered and well ordered Fe_2O_3 samples. Water was admitted at t=0. The traces reflect the periods of EB admission.

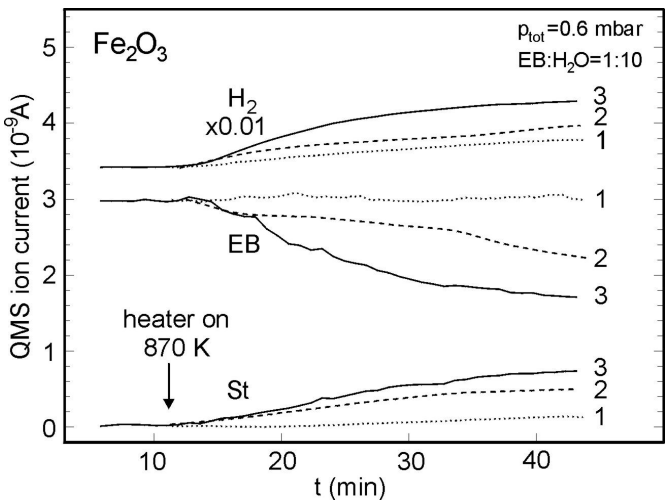

Fig. (2.8).

Mass spectrometric analysis of a batch reactor experiment at intermediate pressure conditions as indicated for three Fe_2O_3 model catalysts with differing surface quality. (1) well ordered, (2) intermediate order, (3) poorly ordered.

2.4 Aims and work strategy

Here, we apply the model catalysis approach to the investigation of the catalytic dehydrogenation of ethylbenzene (EB) to styrene (St) one of the 10 most important catalysed organic reactions, which industrially is performed over potassium-promoted iron oxide catalysts. The reaction is endothermic (ΔH=125 kJ/mol) and is run at high temperature, typically 870 K and at 1 bar in the presence of excess overheated steam.

The aim of this work is based on studying the catalytic activity near to real catalysis conditions over the iron oxide model catalysts, which is the continuation of the work which has been done in our group, through which the growth and characterization of the unpromoted iron oxide phases (FeO, Fe_3O_4 and Fe_2O_3) and the potassium promoted iron oxides (KFe_xO_y) where studied extensively and the different phases were well identified. The adsorption properties and catalytic activity at low and medium pressures were also studied.

The basic idea as we apply it here is to prepare well defined model catalyst samples and to characterize their surface structure and composition under UHV condition using mainly LEED and AES. Then the samples are transferred under vacuum into a reactor which allows to determine the catalytic properties (conversion, selectivity, deactivation behaviour) in-situ under realistic temperature and pressure conditions using a single crystal micro flow reactor. After that, the samples are transferred back into the main UHV chamber for post-reaction analysis.

Our aim is with the help of surface science techniques to

- Identify the phase and structure changes of the catalyst under the course of reaction. The effect and role of steam in the reaction.
- Understand of the main reasons for the deactivation process and how to prevent them.
- Understand the role of iron oxide, promoting effect of potassium and the effect of potassium loading on the activity and deactivation of the catalyst.

The micro flow reactor is designed in a stagnation point form, which allows also the simulation of the reactor and the reaction. This will be done in cooperation with A. Schüle and G. Kolios from the University of Stuttgart.

In addition, the reaction behaviour is studied over pressed powder samples in the micro flow reactor, under the same conditions like the model catalyst. Through comparing the results, information about the diffusion and transport diffusion limitations can be gained. In this way the pressure and material gaps are bridged.